Design and pharmacology of a highly specific dual FMS and KIT kinase inhibitor

Chao Zhang[a,1], Prabha N. Ibrahim[a], Jiazhong Zhang[a], Elizabeth A. Burton[a], Gaston Habets[a], Ying Zhang[a], Ben Powell[a], Brian L. West[a], Bernice Matusow[a], Garson Tsang[a], Rafe Shellooe[a], Heidi Carias[a], Hoa Nguyen[a], Adhirai Marimuthu[a], Kam Y. J. Zhang[a], Angela Oh[a], Ryan Bremer[a], Clarence R. Hurt[a], Dean R. Artis[a], Guoxian Wu[a], Marika Nespi[a], Wayne Spevak[a], Paul Lin[a], Keith Nolop[a], Peter Hirth[a], Greg H. Tesch[b], and Gideon Bollag[a,1]

[a]Plexxikon Inc., Berkeley, CA 94710; and [b]Department of Nephrology, Monash Medical Centre, Monash University, Clayton, VIC 3168, Australia

Edited by Sung-Hou Kim, University of California, Berkeley, CA, and approved February 12, 2013 (received for review November 9, 2012)

Inflammation and cancer, two therapeutic areas historically addressed by separate drug discovery efforts, are now coupled in treatment approaches by a growing understanding of the dynamic molecular dialogues between immune and cancer cells. Agents that target specific compartments of the immune system, therefore, not only bring new disease modifying modalities to inflammatory diseases, but also offer a new avenue to cancer therapy by disrupting immune components of the microenvironment that foster tumor growth, progression, immune evasion, and treatment resistance. McDonough feline sarcoma viral (v-fms) oncogene homolog (FMS) and v-kit Hardy-Zuckerman 4 feline sarcoma viral oncogene homolog (KIT) are two hematopoietic cell surface receptors that regulate the development and function of macrophages and mast cells, respectively. We disclose a highly specific dual FMS and KIT kinase inhibitor developed from a multifaceted chemical scaffold. As expected, this inhibitor blocks the activation of macrophages, osteoclasts, and mast cells controlled by these two receptors. More importantly, the dual FMS and KIT inhibition profile has translated into a combination of benefits in preclinical disease models of inflammation and cancer.

cancer bone metastasis | CSF1R | rheumatoid arthritis | scaffold-based drug design

Deregulated signaling networks are responsible for many human diseases, and our improved understanding of cellular circuitry has led to targeted therapeutics that focus on specific molecular drivers. Kinases have been one of the most intensively explored families of drug targets in cancer over the past two decades, and 17 small-molecule kinase inhibitors have been approved for oncology indications since 2001 (Table S1). In addition, kinase inhibitors for the treatment of rheumatoid arthritis (RA) and other autoimmune diseases have progressed to phase-3 clinical trials (1). Tofacitinib (2), a JAK kinase inhibitor that was recently approved by the Food and Drug Administration for the treatment of moderate-to-severe active RA, was the first new oral disease-modifying antirheumatic drug in more than a decade. It is anticipated that kinase inhibitors will also be found suitable for the treatment of other disorders.

McDonough feline sarcoma viral (v-fms) oncogene homolog (FMS, also known as CSF1R), first discovered as the oncogene responsible for feline McDonough sarcoma (3), is a member of the platelet-derived growth factor receptor (PDGFR) family of class-III receptor tyrosine kinases (RTKs). The two known ligands of FMS, macrophage colony-stimulating factor (M-CSF or CSF-1) (4) and interleukin 34 (IL-34) (5), activate signaling through the receptor in a similar fashion (6, 7) but differ in their developmental and tissue-specific expression patterns (8). Ligand-stimulated FMS tyrosine phosphorylation regulates the survival, proliferation, and differentiation of monocyte/macrophage lineages (9). Macrophages, microglia, and osteoclasts play important roles in inflammatory processes (10), and tumor-associated macrophages are increasingly recognized as a driving force for tumor progression and metastasis (11) and resistance to chemo- and radiotherapy (12, 13). Thus, the inhibition of FMS kinase activity has great potential in treating bone osteolysis and inflammation as well as cancers promoted by macrophages (14).

The stem cell factor (SCF) receptor v-kit Hardy-Zuckerman 4 feline sarcoma viral oncogene homolog (KIT) (15) is another member of the PDGFR family [the other three members are PDGFRα, PDGFRβ, and fms-related tyrosine kinase 3 (FLT3)]. Mutational activation of KIT has been well-documented in a number of cancers (16–18). Tumor control due to blockade of oncogenic KIT mutations has been validated in the clinic through the established efficacy in gastrointestinal stromal tumors of the multikinase inhibitors imatinib and sunitinib (19, 20), which inhibit KIT, among other kinases. In addition, bone marrow-derived cells that depend on the activation of KIT, particularly mast cells, are required in the tumor microenvironment to promote the growth of certain tumors (e.g., neurofibromin 1–dependent tumors and pancreatic ductal adenocarcinoma) (21, 22). Like macrophages, SCF-mediated mast cell infiltration and activation exacerbate inflammation and immunosuppression in the tumor microenvironment. Tryptase, a specific mast-cell protein, has been described as a prognostic marker for survival outcome and thus could serve as a patient stratification biomarker.

We pursued a strategy of combined inhibition of FMS and KIT because of the multiple potential therapeutic opportunities it presents. In addition to cancer, dual FMS and KIT inhibitors are expected to control inflammatory diseases such as RA. Inhibition of FMS is expected to reduce monocyte maturation and osteoclastogenesis (23). Blocking KIT activation is expected to induce mast-cell apoptosis, thereby reducing the production of inflammatory cytokines and degradative molecules in the synovium (24). Imatinib, which inhibits several tyrosine kinases, showed efficacy in the treatment of RA (25, 26). However, imatinib has a limited therapeutic window owing to its modest kinase selectivity. A highly specific inhibitor of FMS and KIT is likely to deliver on this clinical promise with fewer toxicity concerns.

Scaffold-based drug discovery is particularly suited to deriving drugs with desired biological profiles (27–29). Previously, we have identified a 7-azaindole scaffold through a low-affinity, low-selectivity, low-molecular-weight screen and used it to rationally design highly selective BRAF (v-raf murine sarcoma viral oncogene homolog B1) inhibitors that target the oncogenic form of the protein (28). The optimized lead, vemurafenib (30), was the first FDA-approved drug discovered by this approach (31). Here

PHARMACOLOGY

Author contributions: C.Z., P.N.I., P.H., G.H.T., and G.B. designed research; J.Z., E.A.B., G.H., Y.Z., B.P., B.L.W., B.M., G.T., R.S., H.C., H.N., A.M., K.Y.J.Z., A.O., R.B., C.R.H., G.W., M.N., W.S., and G.H.T. performed research; J.Z., B.P., B.L.W., G.T., R.S., H.C., H.N., R.B., C.R.H., G.W., and M.N. contributed new reagents/analytic tools; C.Z., P.N.I., E.A.B., G.H., Y.Z., B.M., K.Y.J.Z., D.R.A., W.S., P.L., K.N., P.H., G.H.T., and G.B. analyzed data; and C.Z. and G.B. wrote the paper.

The authors declare no conflict of interest.

This article is a PNAS Direct Submission.

Data deposition: The atomic coordinates and structure factors have been deposited in the Protein Data Bank, www.pdb.org (PDB ID codes 4HVS and 4HW7).

[1]To whom correspondence may be addressed. E-mail: CZhang@plexxikon.com or gbollag@plexxikon.com.

This article contains supporting information online at www.pnas.org/lookup/suppl/doi:10.1073/pnas.1219457110/-/DCSupplemental.

we show that by exploring a different strategy to fulfill a key hydrogen bond interaction we have generated a second series of 7-azaindole–derived compounds that show highly specific inhibition of both FMS and KIT. As expected, the inhibitor blocks the activation of macrophages, osteoclasts, and mast cells controlled by these two receptors. More importantly, the dual FMS and KIT inhibition profile leads to combined benefit in preclinical disease models of inflammation and cancer bone metastasis.

Results

Scaffold-Based Design of PLX647. 7-Azaindole was identified as a unique kinase inhibitor scaffold through a scaffold discovery campaign that used low-affinity enzymatic screening of more than 20,000 low-molecular-weight compounds against multiple kinases followed by crystallographic characterization of the screening hits (28, 32). The scaffold itself showed multiple binding poses when it was first crystallized with the PIM1 kinase (a kinase with an atypical ATP-binding pocket), but it assumed a single binding mode once substitution on the 3- position was added to interact with the kinase selectivity pocket adjoining the gatekeeper residue. An early analog, 3-(3-methoxylphenyl-methyl)-7-azaindole (PLX070), cocrystallized with fibroblast growth factor receptor 1 (FGFR1), revealed a key interaction between the ether oxygen and the backbone NH of the aspartate residue of the conserved Asp-Phe-Gly (DFG) motif (Fig. 1) (28). In developing BRAF inhibitors, we replaced the methoxy group with a sulfonamide alkyl tail to better access the interior pocket unique to the mutant BRAF protein (Fig. 1). To craft the sulfonamide nitrogen into a hydrogen bond acceptor (i.e., a stronger acid), the phenyl middle ring was rendered electron-deficient by fluorine substitutions at the 2- and 6- positions. In addition, the original methylene linker was replaced by a keto group to maintain the near coplanarity of the linker-azaindole geometry.

In a separate series, we kept the 3-methylene linker of PLX070 and used pyridine as the middle ring to afford the endocyclic nitrogen as the hydrogen bond acceptor in place of the exocyclic ether oxygen. This series, represented by PLX647 (Fig. 1), yields potent inhibitors of both FMS and KIT that show strong selectivity compared with other kinases (discussed below). In the in vitro enzymatic assay, PLX647 inhibits FMS with IC_{50} = 0.028 μM and KIT with IC_{50} = 0.016 μM.

We determined the crystal structure of PLX647 in complex with KIT and the structure of the 5-methoxyl analog of PLX647 (dubbed here PLX647-OMe) in complex with FMS. PLX647-OMe is a slightly less potent inhibitor of FMS (IC_{50} = 0.062 μM) than PLX647 but has better aqueous solubility (solubility is 14 μM for PLX647 and 77 μM for PLX647-OMe based on a turbidity-based assay) and was thus more suitable for cocrystallization with FMS. Because the difference between the two compounds lies in the solvent-accessible 5-substitution on the 7-azaindole, the structure of FMS/PLX647-OMe complex is representative of the interactions formed between PLX647 and FMS.

In its complex with the KIT kinase, PLX647 binds to the autoinhibited state of the protein (Fig. 1) with the juxtamembrane domain [the region between the transmembrane helix and the cytoplasmic kinase domain (33)], preventing the activation loop from adopting the so-called DFG-in conformation (a state in which the phenylalanine side chain of the DFG motif is buried inside and away from the ATP-binding pocket). In particular, the juxtamembrane domain residue Trp557 of KIT forms part of the inhibitor binding surface. Although PLX647-OMe also binds the DFG-out conformation of FMS, the juxtamembrane domain of FMS is displaced by the inhibitor and not visible in the structure (Fig. 1). The juxtamembrane domain of KIT, which was included in the expression construct (residues 551–582), was well defined in the electron densities of the KIT–PLX647 cocrystal. The N-terminal inhibitor binding region is >8 Å away from the closest neighboring molecule. Therefore, the interaction between the juxtamembrane domain and PLX647 is unlikely a result of the crystal packing. In the FMS–PLX647-OMe crystal, although the N-terminal region of the juxtamembrane domain is displaced by the inhibitor, the vacant space is not occupied by any neighboring molecule. In fact, a crystal structure of the apo-FMS protein obtained using the same construct and crystallization condition shows clear electron density for the N-terminal region of the juxtamembrane domain. Therefore, the N-terminal region of the juxtamembrane domain has room to adjust its conformation in response to inhibitor binding, and the difference in conformations of the juxtamembrane domains in KIT and FMS is not caused by interactions involved in crystal packing.

The trifluoromethyl-phenylmethylamino tails of PLX647 and PLX647-OMe adopt slightly different orientations in the two complexes (Fig. S1), correlating to different states of the juxtamembrane domains in the two enzymes. Beyond the gatekeeper residues (Thr663 in FMS and Thr670 in KIT), the kinase selectivity pockets of the two proteins differ by only one residue,

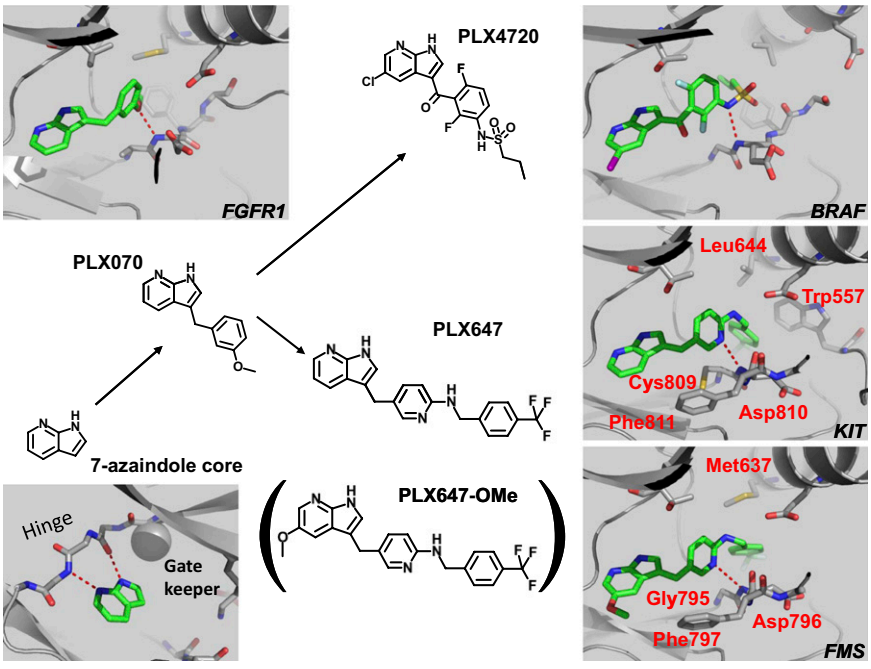

Fig. 1. Scaffold-based discovery of PLX647 and structural basis of its dual-binding specificity. Two chemical series were derived from the 7-azaindole scaffold. They represent different strategies for realizing a hydrogen bond interaction with the backbone NH group of the DFG motif.

Met637 in FMS and Leu644 in KIT. A more significant difference between FMS and KIT lies in the residue preceding the DFG motif, which is glycine (Gly795) in FMS and cysteine (Cys809) in KIT (Fig. 1). Although this residue does not make direct contact with the trifluoromethyl-phenylmethylamino tail, in KIT the large side chain of Cys809 pushes the pyridine toward the gatekeeper Thr670, affecting the tail orientation indirectly (Fig. S1). Structurally, Gly795 and Cys809 serve as the "lower gatekeeper" to the selectivity pockets of FMS and KIT, respectively.

Cellular Pharmacology. Ba/F3 cells are mouse pro-B cells that depend on IL-3 for survival. Engineering Ba/F3 cells to express breakpoint cluster region (BCR)-activated kinase replaces dependence on IL-3 with the constitutive activity of the kinase (34). Consequently, the survival of BCR–FMS- and BCR–KIT-expressing Ba/F3 cells is dependent on FMS and KIT kinase activities, respectively. In vitro, proliferation of BCR–FMS cells was potently inhibited by PLX647, with an IC_{50} of 0.092 μM. A corresponding Ba/F3 cell line expressing BCR–KIT was also quite sensitive to PLX647, with an IC_{50} of 0.18 μM. However, PLX647 did not inhibit the proliferation of these Ba/F3 cell lines when IL-3 was present, confirming the selective inhibition by PLX647 of the introduced kinase. PLX647 also inhibits endogenous FMS and KIT, as demonstrated by inhibition of the ligand-dependent cell lines M-NFS-60 (IC_{50} = 0.38 μM) and M-07e (IC_{50} = 0.23 μM), which express FMS and KIT, respectively. PLX647 did not reduce the viability of 293T kidney cells or HepG2 hepatocellular carcinoma cells at a 50 μM concentration, suggesting that the effect of PLX647 on cellular proliferation was due to its ability to selectively inhibit FMS and KIT.

Human osteoclast precursor cells require the combination of colony-stimulating factor 1 (CSF-1) and receptor activator of nuclear factor kappa-B ligand (RANKL) to differentiate into mature osteoclasts (35, 36). The production of mature osteoclasts from osteoclast precursors can be examined by quantifying the amount of acid phosphatase in the culture media, resulting from secretion of tartrate-resistant acid phosphatase 5b (TRAP5b) by the mature osteoclasts (37). Using this method, PLX647 was shown to inhibit osteoclast differentiation with an IC_{50} of 0.17 μM (Table S2).

Kinase Selectivity. PLX647 was tested against a panel of 400 kinases at a concentration of 1 μM, 35-fold above its FMS enzymatic IC_{50} and 60-fold above its KIT enzymatic IC_{50}. In addition to FMS and KIT, the activities of only nine kinases were inhibited by more than 50% (Table S3). Subsequent IC_{50} determination showed that IC_{50}s for FLT3 and kinase insert domain receptor (KDR) were 0.091 μM and 0.13 μM, respectively. All other kinases tested showed IC_{50} >0.3 μM (Table S3).

To evaluate the ability of PLX647 to inhibit FLT3 in a cellular context, we tested whether PLX647 was able to block the growth of the human FLT3-dependent leukemic cell lines OCI-AML5 and MV4-11, which express either wild-type FLT3 or an internal tandem duplication mutant of FLT3 (FLT3-ITD (38)), respectively. PLX647 potently inhibits the growth of FLT3–ITD-expressing MV4-11 cells (IC_{50} = 0.11 μM) but not OCI-AML5 (IC_{50} = 1.6 μM), which express wild-type FLT3. The lack of inhibition of wild-type FLT3 cells suggests that PLX647 binds only weakly to unactivated FLT3 and the IC_{50} measured using isolated enzyme may not be biologically relevant. In contrast, PLX647 may be effective against cancers such as acute myeloid leukemia that are transformed by FLT3–ITD.

PLX647 displayed minimal inhibition of the proliferation of Ba/F3 cells expressing BCR–KDR (IC_{50} = 5 μM). This correlates with the equally weak inhibition of vascular endothelial growth factor (VEGF)-stimulated human umbilical vein endothelial cells (HUVECs) (IC_{50} = 3.0 μM) (Table S2). Together, these data suggest that PLX647 lacks appreciable inhibition of cellular KDR2.

Pharmacological Characterization of PLX647 in Rodents. To characterize the pharmacology of PLX647, we used rodent models of LPS-induced cytokine release, mast cell activation, kidney inflammation, collagen-induced arthritis, and cancer-induced bone pain and osteolysis. The FMS and KIT kinase domains in the human, mouse, and rat are highly homologous. (Fig. S2). Although the lack of sufficient amounts of recombinant mouse and rat receptors has precluded us from directly measuring the IC_{50}s of PLX647 against rodent FMS and KIT, the potencies are expected to be very similar to what was measured for the human enzymes. This is supported by the fact that M-NFS-60, a murine myeloblastic leukemia cell line whose growth depends on FMS, is as sensitive to PLX647 as human cell lines (THP-1, Table S2).

The pharmacokinetics of PLX647 were characterized in mice and rats. Intravenous administration of PLX647 in mice and rats at 2 mg/kg showed moderate systemic clearance and a high volume of distribution (Table 1). Following oral administration of PLX647 at 10 or 40 mg/kg, systemic exposures in the mouse and rat both increased in a dose-related, slightly greater than dose-proportional manner, with mean bioavailability (*F*) between 45% and 81%. The systemic exposures of PLX647 in mice and rats with area under the concentration curve (AUC) ranging from 6,400 h·ng/mL (or 270 μM·h) to 53,300 h·ng/mL (or 2,200 μM·h) translate into an average plasma concentration from 0.5 to 6 μM, corresponding approximately to the cellular IC_{50} and IC_{90}, respectively. Therefore, PLX647 doses used in the in vivo models described below produce concentrations in the proper range for observing the pharmacologic effects of FMS and KIT inhibition.

Effect on LPS-Induced TNF-α and IL-6 Release. We determined the effects of FMS inhibition by PLX647 on LPS-induced cytokine induction. LPS injection in mice results in elevation of inflammatory cytokines, including TNF-α and IL-6, which peak at 1.5 and 1.5–2.5 h postinjection, respectively. PLX647 (40 mg/kg) was dosed orally 4.25 h before LPS injection. Treatment with PLX647 reduced serum TNF-α levels by 85% compared with the vehicle control (Fig. S3*A*). In the same experiment, the positive control dexamethasone (0.5 mg/kg, PO) lowered the TNF-α levels by 96%. Treatment with 40 mg/kg PLX647 also resulted in significant inhibition of IL-6 release (75%), with similar potency to dexamethasone (70%) (Fig. S3*B*).

Effect on Mast Cell Activation in Skin. Passive cutaneous anaphylaxis (PCA) is a well-established experimental method for assessing mast cell activation in skin (39). At an 80 mg/kg dose, PLX647 inhibited mast cell degranulation by 38% in a mouse PCA model (Fig. S4). KIT has a central role in mast cell development and function, and stimulation by SCF causes antigen-dependent mast cell degranulation, suggesting that inhibition of the PCA reaction by PLX647 is a pharmacological response to KIT inhibition. It should be noted that the degranulation stimulus used in this study was IgE, relying on endogenous KIT ligand present to activate KIT and prime IgE signaling. Partial inhibition of PCA

Table 1. Summary of pharmacokinetic parameters of PLX647

	Intravenous					Oral gavage*	
Species	Dose, mg/kg	$AUC_{0-\infty}$, h·ng/mL	CL, mL·min^{-1}·kg^{-1}	Vss, L/kg	$t_{1/2}$, h	10 mg/kg	40 mg/kg
Mouse	2	3,750	8.91	1.76	2.29	8,510/1,670 (*F* = 45%)	53,300/7,780 (*F* = 71%)
Rat	2	2,850	11.7	2.14	2.16	6,400/630 (*F* = 45%)	46,350/3,720 (*F* = 81%)

AUC, area under the concentration-time curve; CL, clearance; *F*, percentage oral bioavailability; $t_{1/2}$, terminal half life; Vss, volume of distribution at steady state.
*$AUC_{0-\infty}$ (h·ng/mL)/C_{max} (ng/mL), percentage of bioavailability in parentheses.

may be the maximum effect achievable by a KIT inhibitor in this IgE-driven system.

Effect on Acute Kidney Inflammation. Next, we tested whether PLX647 could suppress kidney macrophage proliferation in an acute mouse model of renal inflammation induced by unilateral ureter obstruction (UUO) (40). In contrast to the nonligated kidneys, there were profound tubulointerstitial lesions in the renal cortexes of all UUO kidneys on day 7. Quantitative immunostaining analysis identified a marked accumulation of interstitial F4/80+ macrophages in the UUO kidneys to levels 6- to 10-fold higher than those observed in nonligated kidneys (Fig. 2 *A* and *C*). Treatment with vehicle alone caused a small but significant increase in the macrophage levels in the nonligated kidney (Fig. 2*C*). In the UUO kidneys, treatment with PLX647 [40 mg/kg twice daily (BID)] resulted in reduction in the levels of F4/80+ macrophages by 77% compared with vehicle (Fig. 2 *B* and *C*). The macrophage levels achieved in the UUO kidneys treated with PLX647 were not statistically different from those in the nonligated kidney treated with vehicle alone, suggesting that PLX647 was substantially effective in preventing macrophage accumulation in UUO kidneys.

Double immunostaining showed that significant numbers of F4/80+ macrophages in the UUO kidneys of vehicle groups also expressed the proliferating nuclear antigen Ki67, indicating that these macrophages were proliferating locally within the obstructed kidney (Fig. 2*A*). In comparison, proliferating macrophages (F4/80+ Ki67+ cells) were rarely detected in the UUO kidneys of mice treated with PLX647, which were similar to the nonligated kidneys treated with vehicle alone (Fig. 2*B*). This suggests that PLX647 inhibited macrophage accumulation in UUO kidneys, in part, by suppressing kidney macrophage proliferation.

At the end of the 7-d UUO experiment, the proportion of CD68+ blood monocytes was the same in nontreated and vehicle-treated mice. However, the blood monocyte levels were reduced by 65% in mice that had received 7 d of PLX647 treatment (Fig. 2*D*).

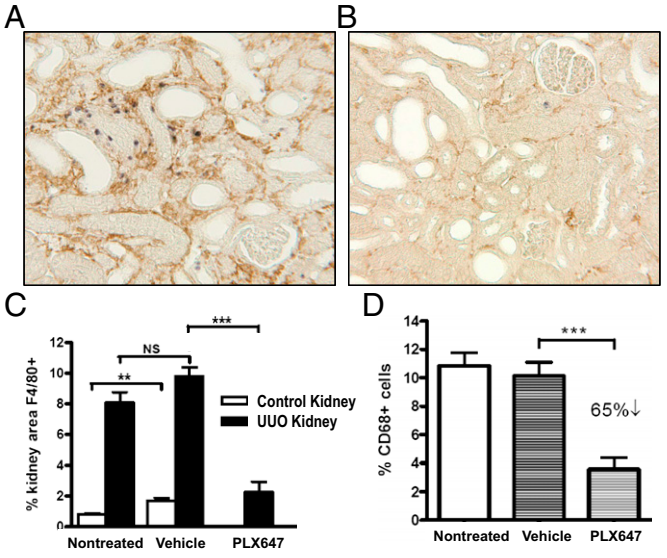

Fig. 2. PLX647 reduces macrophage accumulation in UUO kidney and blood monocytes. (*A*) Immunostaining identified large numbers of interstitial F4/80+ macrophages (brown) in the UUO kidney of a vehicle-treated mouse, and a significant proportion of these macrophages expressed the Ki67 antigen (blue) in their nuclei, indicating that they were proliferating. (*B*) Macrophage accumulation and proliferation was substantially reduced in the UUO kidneys of mice treated with PLX647. (*C*) Immunostaining was used to assess the accumulation of F4/80+ macrophages in mouse kidneys. Compared with nonligated control kidneys, UUO kidneys showed a 6- to 10-fold increase in the area of renal cortex containing macrophages at day 7. Treatment with PLX647 reduced the macrophage levels in UUO kidneys to a level similar to that found in control kidneys. (*D*) Peripheral blood monocytes from UUO mice were purified by density centrifugation and assessed for CD68 expression by flow cytometry. Treatment with PLX647 for 7 d reduced circulating blood monocytes by 65% (**$P < 0.01$, ***$P < 0.001$).

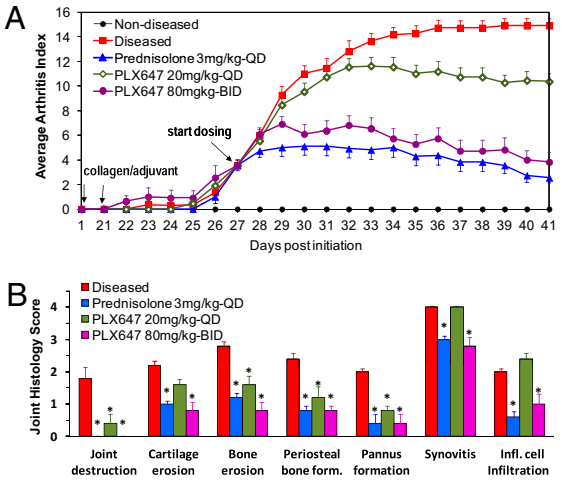

Fig. 3. The effect of PLX647 on mouse CIA. (*A*) Clinical arthritic scores over the course of disease induction and treatment. After a second collagen/adjuvant emulsion injection on day 21, the mice were scored daily for signs of arthritis. One of the five possible scores was assigned for each limb: 0 = no visible effects of arthritis, 1 = edema and/or erythema of one digit, 2 = edema and/or erythema of two joints, 3 = edema and/or erythema of more than two joints, and 4 = severe arthritis of the entire paw and digits. The final score for each animal was the sum of the scores for all four limbs (ranging from 0 to 16). (*B*) Effect of disease and treatment on joint histology. The histology of the joint was graded using the following scores: 0, normal; 1, minimal; 2, mild; 3, moderate; and 4, severe. Treatment groups that showed significant changes ($P < 0.05$) relative to the vehicle-treated disease control are indicated by an asterisk.

Effect on Collagen-Induced Arthritis. PLX647 was tested in a chronic model of mouse collagen-induced arthritis (CIA) (41). Collagen/adjuvant emulsion was injected into the tails of mice on days 1 and 21 of the study. The first signs of arthritis were observed on day 22 (Fig. 3*A*). By day 27, a sufficient number of animals had signs of arthritis to initiate treatment. Maximum severity of arthritis for the disease control group was observed on day 39. Oral administration of a daily dose of 3 mg/kg prednisolone initially delayed the continued development of severe arthritic symptoms, relative to vehicle-treated diseased animals. By day 35, the signs of arthritis began to decrease in this treatment group, reaching a maximal reduction in disease score of 85%, relative to the vehicle-treated diseased animals, on day 41 (Fig. 3*A*).

Oral administration of a daily dose of 20 mg/kg PLX647 had no initial effect on the development of severe arthritis. However, starting on day 33, no further development of disease severity was recorded, and a 30% inhibition of the macroscopic signs of arthritis was evident in clinical score on day 41. Like the group treated with 3 mg/kg prednisolone, mice treated with 80 mg/kg BID PLX647 initially showed delayed development of severe arthritic signs. Starting on day 33, the signs of arthritis began to decrease in this treatment group, reaching a maximum reversal of 76% on day 41 (Fig. 3*A*).

Histological examination at the end of study showed that the limbs from diseased mice were enlarged, with mild inflammatory cell infiltration into the soft tissue. These joints had mild joint destruction, moderate cartilage and bone erosion, moderate periosteal bone and pannus formation, and severe synovitis. Most of these histological parameters were inhibited by PLX647 in a dose-dependent manner (Fig. 3*B*). There was a total absence of bone destruction in the high-dose PLX647 group and the prednisolone group. Although low-dose PLX647 showed no effect on inflammatory cell infiltration and synovitis, both 3mg/kg prednisolone and 80 mg/kg BID PLX647 significantly reduced the inflammatory cell infiltration of the soft tissue (by 70% and 50%, respectively) and inhibited synovitis relative to the disease control group (Fig. 3*B*).

Effect on Cancer-Induced Bone Pain and Osteolysis. PLX647 was also evaluated using a syngeneic rat model of cancer-induced bone pain (42). After intratibial injection of MRMT-1 mammary gland tumor cells in rats, significant allodynia developed in the MRMT-1 inoculated animals by day 10 and they remained allodynic on day 14 (testing day). Treatment with 5 mg/kg morphine was able to completely reverse the allodynia. Administration of 30 mg/kg BID PLX647 also induced a significant reversal of allodynia on day 14 compared with the vehicle group (Fig. 4*A*). In the histological evaluation, PLX647 treatment resulted in significant inhibition of TRAP5b immunostaining and bone osteolysis (Fig. 4*B*). As demonstrated by the representative micro-computerized tomography images, 30 mg/kg BID PLX647 was able to prevent bone damage by the tumor cells (Fig. 4*C*). In contrast, morphine had no protective effect on the bone.

Discussion

PLX647 represents a unique class of kinase inhibitors with unique dual FMS and KIT specificity. PLX647 was derived from the same 7-azaindole scaffold that was used to develop vemurafenib, the first-in-class BRAF inhibitor approved for late-stage metastatic melanoma (31). Together, these examples illustrate how a nonspecific, low-affinity scaffold occupying the common space in the kinase active site has the potential to be a multifaceted progenitor: A single scaffold can thus give rise to multiple chemical series exhibiting different pharmacological profiles.

In its complexes with FMS and KIT, the middle ring pyridine nitrogen of PLX647 forms a hydrogen bond to the backbone NH of the respective DFG aspartate (Asp796 of FMS or Asp810 of KIT). This interaction depends critically on the conformational flexibility of the methylene linker in PLX647, because the keto linker analog exhibits a >100-fold loss in potency ($IC_{50} > 5\mu M$ in FMS and KIT enzymatic assays). Such an interaction has not been observed in previously published structures of kinase-inhibitor complexes. The high selectivity of PLX647 against other kinases suggests that the large majority of the kinome do not allow the pyridine to access the backbone NH in this fashion.

PLX647 binds to the auto-inhibited state of FMS and KIT, and in the case of KIT, the juxtamembrane domain (in particular Trp557) constitutes part of the binding interface. A small number of receptor tyrosine kinases (e.g., ephrin receptors, MUSK, and PDGFRs) share this juxtamembrane domain-mediated autoinhibition mechanism, although the details of the interactions are different. For example, FLT3, the closest human homolog to FMS and KIT, contains a leucine (Leu576) instead of tryptophan in the juxtamembrane domain. We compared the binding mode of PLX647 in KIT to that of sunitinib and imatinib, both inhibiting FMS and KIT and a spectrum of other kinases (Fig. S5). Although sunitinib also binds to the auto-inhibited state, it does not enter the kinase selectivity pocket and, thus, sunitinib makes no direct contact with any juxtamembrane domain residues. Imatinib, however, completely displaces the juxtamembrane domain. As a result of this conformation-specific binding, the PLX647 class of inhibitors is expected to exhibit distinctive biological activity that may translate into improved efficacy and safety in the clinic. Ki20227, which was initially reported as a FMS inhibitor (43), seemed to inhibit both FMS and KIT in our assays (IC_{50} = 0.023 μM for both kinases). Ki20227 also showed in vivo efficacy in mouse models of cancer-induced osteolytic bone destruction (43) and CIA (44). It will be interesting to compare the binding of PLX647 and Ki20227 when the costructures of the latter with FMS and KIT are obtained.

PLX647 was evaluated in a number of pharmacological models. PLX647 selectively blocks the proliferation, migration, and activation of macrophages, osteoclasts, and mast cells, the three main cell populations controlled by FMS and KIT. In the UUO model of acute kidney inflammation, macrophage accumulation is largely dependent on local proliferation facilitated by increased CSF-1 production in the injured kidney (40). In UUO kidneys, PLX647 reduced both the proliferation and accumulation of macrophages. In addition, PLX647 reduced the number of blood monocytes that are available to be recruited into the injured kidney, presumably by suppressing the FMS-dependent proliferation of monocyte precursor cells in the bone marrow.

In a mouse collagen-induced arthritis model, PLX647 inhibited all parameters of disease progression in a dose-dependent manner. This included clinical arthritic score, cartilage damage, bone erosion, periosteal bone formation, synovitis, pannus formation, joint destruction, and cell infiltration in soft tissue. The effect of PLX647 at 80 mg/kg BID was comparable to prednisolone at 3 mg/kg given once daily (QD). These results suggest that PLX647 targets both bone destruction and inflammatory components of collagen-induced arthritis through inhibition of FMS and KIT activity.

Osteoclasts require the simultaneous stimulation of the RANKL and FMS pathways for differentiation, activity and survival (35, 36). Recently, RANKL antagonists have demonstrated efficacy to prevent bone destruction in preclinical models, and one such antibody, denosumab, is now an approved therapeutic (45). As a potent inhibitor of FMS, the anti-osteoclast effects of PLX647 that are seen in vitro and in vivo provide an alternative mechanism to block bone and joint destruction and consequent pain.

Bone is the third most common site of metastases after lung and liver and is the primary site of metastatic disease in patients with breast, prostate, and lung cancer (46). The bone lesions that result from metastatic disease also cause severe bone pain, which is a major clinical problem in cancer patients. The results of this study show that PLX647 has analgesic efficacy in the cancer-induced bone pain model. Unlike conventional analgesics, PLX647 may affect the underlying disease and protect bone from damage by osteolytic tumor cells.

Finally, dual FMS and KIT inhibitors such as PLX647 have the potential to reprogram the immune microenvironment in tumors and thus represent a promising strategy for improving the efficacy of anticancer treatments. For example, tumor associated macrophages (TAMs) promote tumor progression by stimulating tumor vascularization, invasion, and metastasis. Just as PLX647 has demonstrated efficacy in inflammation models by depleting infiltrating macrophages, its sister compound PLX3397 has sensitized tumors to standard chemotherapy by depleting infiltrating TAMs in a mouse breast cancer model (13). Accordingly, PLX3397, which has completed phase-1 testing in solid tumor patients, is currently undergoing clinical evaluation in a number of cancer indications.

With improved kinome selectivity, the PLX647 class of inhibitors are expected to have a better safety profile than more promiscuous kinase inhibitors such as imatinib and sunitinib. However, both FMS and KIT regulate a number of important

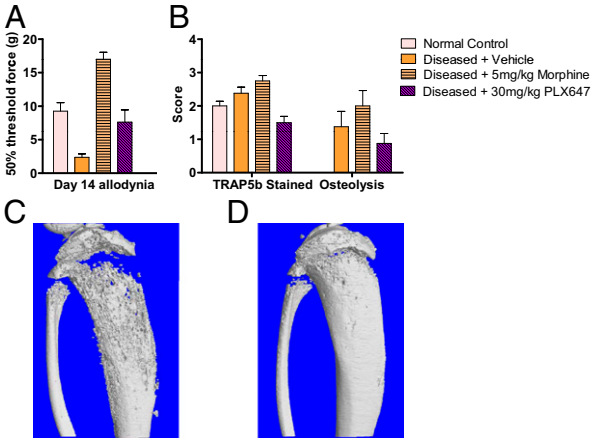

Fig. 4. PLX647 inhibits cancer bone pain and osteolysis. (*A*) Significant allodynia developed in the MRMT-1 inoculated animals at day-14 testing. PLX647 showed a significant reversal of allodynia compared with the vehicle group ($P < 0.01$). (*B*) Bone histopathology results of TRAP5b staining and osteolysis measures. Histopathology scoring criteria: 0, normal; 1, mild; 2, moderate; and 3, severe. (*C* and *D*) Representative micro-computerized tomography scans of the proximal ends of the tibiae of rats receiving MRMT-1/vehicle-po/saline-sc and MRMT-1/PLX647-po/saline-sc. PLX647 30 mg/kg BID protects rat from cancer-induced bone erosion.

cellular functions and some target-related toxicity is anticipated based on the known pharmacology of FMS and KIT inhibition. It is important to understand the risk of such potential toxicities and monitor them closely during the development of these inhibitors to ensure that clinical benefit significantly outweighs the risk. Targeted ablation of Fms in mice resulted in severe osteopetrosis, compromised immunity, reproductive defects, and perturbations in the development of other organs (47), whereas Kit-deficient mice showed abnormalities in germ-cell development and melanogenesis, which resulted in unpigmented skin, in addition to hematopoietic defects (48). Although some of these phenotypes are developmental, the mouse knockouts should be useful to predict toxicities in further preclinical and clinical studies.

Experimental Procedures

Detailed methods are included in *SI Experimental Procedures*.

Compound Synthesis. PLX647, 5-(1H-pyrrolo[2,3-b]pyridin-3-ylmethyl)-*N*-[[4-(trifluoromethyl)phenyl]methyl]pyridin-2-amine, was synthesized from commercially available 5-bromopyridin-2-amine, 4-(trifluoromethyl)benzaldehyde and 1H-pyrrolo[2,3-b]pyridine following the synthetic route depicted in Scheme S1 (*SI Experimental Procedures*).

Protein Purification, Crystallization, and Structure Determination. To enable crystallization, the KIT cDNA fragment encoding amino acid residues P551–H934, containing a deletion between (Q694–T753) and 16 surface mutations (I563S, V569S, Y609Q, L631S, M651E, I662H, I690H, C691S, K693D, I756S, L762N, V825D, C844S, L890S, L912D, and L923D) were expressed in *Escherichia coli* cells, and the FMS cDNA fragment encoding amino acid residues Q542–R919, also containing a deletion between (G696–D741), and additional mutations (C667T, C830S, and C907T), were expressed in Sf9 insect cells. Details of protein purification and crystallization are given in *SI Experimental Procedures*. Crystallographic data and refinement statistics are given in Table S4.

Biochemical and Cellular Assays. The in vitro kinase activities were determined by measuring phosphorylation of a biotinylated substrate peptide. Kinome selectivity screen was carried out using commercial kinase profiling service (*SI Experimental Procedures*). Details of cell-based assays to evaluate the ability of PLX647 to inhibit FMS, KIT, FLT3, and KDR catalytic activity in cells are given in *SI Experimental Procedures* and Table S2.

In Vivo Studies. All animal studies were conducted in accordance with the Institute for Laboratory Animal Research Guide for the Care and Use of Laboratory Animals and the US Department of Agriculture Animal Welfare Act. Detailed study designs are given in *SI Experimental Procedures*.

ACKNOWLEDGMENTS. X-ray diffraction data were collected at beamline ALS 8.3.1 at the Advanced Light Source (Lawrence Berkeley Laboratory).

1. Kontzias A, Laurence A, Gadina M, O'Shea JJ (2012) Kinase inhibitors in the treatment of immune-mediated disease. *F1000. Med-Rep* 4:5.
2. Fleischmann R, et al.; ORAL Solo Investigators (2012) Placebo-controlled trial of tofacitinib monotherapy in rheumatoid arthritis. *N Engl J Med* 367(6):495–507.
3. Sherr CJ, et al. (1985) The c-fms proto-oncogene product is related to the receptor for the mononuclear phagocyte growth factor, CSF-1. *Cell* 41(3):665–676.
4. Stanley ER, Cifone M, Heard PM, Defendi V (1976) Factors regulating macrophage production and growth: Identity of colony-stimulating factor and macrophage growth factor. *J Exp Med* 143(3):631–647.
5. Lin H, et al. (2008) Discovery of a cytokine and its receptor by functional screening of the extracellular proteome. *Science* 320(5877):807–811.
6. Liu H, et al. (2012) The mechanism of shared but distinct CSF-1R signaling by the non-homologous cytokines IL-34 and CSF-1. *Biochim Biophys Acta* 1824(7):938–945.
7. Ma X, et al. (2012) Structural basis for the dual recognition of helical cytokines IL-34 and CSF-1 by CSF-1R. *Structure* 20(4):676–687.
8. Wei S, et al. (2010) Functional overlap but differential expression of CSF-1 and IL-34 in their CSF-1 receptor-mediated regulation of myeloid cells. *J Leukoc Biol* 88(3):495–505.
9. Chitu V, Stanley ER (2006) Colony-stimulating factor-1 in immunity and inflammation. *Curr Opin Immunol* 18(1):39–48.
10. Murray PJ, Wynn TA (2011) Protective and pathogenic functions of macrophage subsets. *Nat Rev Immunol* 11(11):723–737.
11. Ruffell B, Affara NI, Coussens LM (2012) Differential macrophage programming in the tumor microenvironment. *Trends Immunol* 33(3):119–126.
12. Ahn GO, et al. (2010) Inhibition of Mac-1 (CD11b/CD18) enhances tumor response to radiation by reducing myeloid cell recruitment. *Proc Natl Acad Sci USA* 107(18):8363–8368.
13. DeNardo DG, et al. (2011) Leukocyte complexity predicts breast cancer survival and functionally regulates response to chemotherapy. *Cancer Discov* 1(1):54–67.
14. El-Gamal MI, Anbar HS, Yoo KH, Oh CH (2012) FMS Kinase Inhibitors: Current Status and Future Prospects. *Med Res Rev*, 10.1002/med.21258.
15. Yarden Y, et al. (1987) Human proto-oncogene c-kit: A new cell surface receptor tyrosine kinase for an unidentified ligand. *EMBO J* 6(11):3341–3351.
16. Furitsu T, et al. (1993) Identification of mutations in the coding sequence of the proto-oncogene c-kit in a human mast cell leukemia cell line causing ligand-independent activation of c-kit product. *J Clin Invest* 92(4):1736–1744.
17. Hirota S, et al. (1998) Gain-of-function mutations of c-kit in human gastrointestinal stromal tumors. *Science* 279(5350):577–580.
18. Carvajal RD, et al. (2011) KIT as a therapeutic target in metastatic melanoma. *JAMA* 305(22):2327–2334.
19. Demetri GD, et al. (2002) Efficacy and safety of imatinib mesylate in advanced gastrointestinal stromal tumors. *N Engl J Med* 347(7):472–480.
20. Goodman VL, et al. (2007) Approval summary: Sunitinib for the treatment of imatinib refractory or intolerant gastrointestinal stromal tumors and advanced renal cell carcinoma. *Clin Cancer Res* 13(5):1367–1373.
21. Staser K, Yang FC, Clapp DW (2012) Pathogenesis of plexiform neurofibroma: Tumor-stromal/hematopoietic interactions in tumor progression. *Annu Rev Pathol* 7:469–495.
22. Chang DZ (2012) Mast cells in pancreatic ductal adenocarcinoma. *OncoImmunology* 1(5):754–755.
23. Paniagua RT, et al. (2010) c-Fms-mediated differentiation and priming of monocyte lineage cells play a central role in autoimmune arthritis. *Arthritis Res Ther* 12(1):R32.
24. Reber L, Da Silva CA, Frossard N (2006) Stem cell factor and its receptor c-Kit as targets for inflammatory diseases. *Eur J Pharmacol* 533(1-3):327–340.
25. Eklund KK, Joensuu H (2003) Treatment of rheumatoid arthritis with imatinib mesylate: Clinical improvement in three refractory cases. *Ann Med* 35(5):362–367.
26. Miyachi K, et al. (2003) Efficacy of imatinib mesylate (STI571) treatment for a patient with rheumatoid arthritis developing chronic myelogenous leukemia. *Clin Rheumatol* 22(4-5):329–332.
27. Card GL, et al. (2005) A family of phosphodiesterase inhibitors discovered by cocrystallography and scaffold-based drug design. *Nat Biotechnol* 23(2):201–207.
28. Tsai J, et al. (2008) Discovery of a selective inhibitor of oncogenic B-Raf kinase with potent antimelanoma activity. *Proc Natl Acad Sci USA* 105(8):3041–3046.
29. Artis DR, et al. (2009) Scaffold-based discovery of indeglitazar, a PPAR pan-active anti-diabetic agent. *Proc Natl Acad Sci USA* 106(1):262–267.
30. Bollag G, et al. (2010) Clinical efficacy of a RAF inhibitor needs broad target blockade in BRAF-mutant melanoma. *Nature* 467(7315):596–599.
31. Bollag G, et al. (2012) Vemurafenib: The first drug approved for BRAF-mutant cancer. *Nat Rev Drug Discov* 11(11):873–886.
32. Kumar A, et al. (2005) Crystal structures of proto-oncogene kinase Pim1: A target of aberrant somatic hypermutations in diffuse large cell lymphoma. *J Mol Biol* 348(1):183–193.
33. Hubbard SR (2004) Juxtamembrane autoinhibition in receptor tyrosine kinases. *Nat Rev Mol Cell Biol* 5(6):464–471.
34. Daley GQ, Baltimore D (1988) Transformation of an interleukin 3-dependent hematopoietic cell line by the chronic myelogenous leukemia-specific P210bcr/abl protein. *Proc Natl Acad Sci USA* 85(23):9312–9316.
35. Lacey DL, et al. (1998) Osteoprotegerin ligand is a cytokine that regulates osteoclast differentiation and activation. *Cell* 93(2):165–176.
36. Yoshida H, et al. (1990) The murine mutation osteopetrosis is in the coding region of the macrophage colony stimulating factor gene. *Nature* 345(6274):442–444.
37. Minkin C (1982) Bone acid phosphatase: Tartrate-resistant acid phosphatase as a marker of osteoclast function. *Calcif Tissue Int* 34(3):285–290.
38. Nakao M, et al. (1996) Internal tandem duplication of the flt3 gene found in acute myeloid leukemia. *Leukemia* 10(12):1911–1918.
39. Wershil BK, Mekori YA, Murakami T, Galli SJ (1987) 125I-fibrin deposition in IgE-dependent immediate hypersensitivity reactions in mouse skin. Demonstration of the role of mast cells using genetically mast cell-deficient mice locally reconstituted with cultured mast cells. *J Immunol* 139(8):2605–2614.
40. Le Meur Y, et al. (2002) Macrophage accumulation at a site of renal inflammation is dependent on the M-CSF/c-fms pathway. *J Leukoc Biol* 72(3):530–537.
41. Brand DD, Kang AH, Rosloniec EF (2004) The mouse model of collagen-induced arthritis. *Methods Mol Med* 102:295–312.
42. Medhurst SJ, et al. (2002) A rat model of bone cancer pain. *Pain* 96(1-2):129–140.
43. Ohno H, et al. (2006) A c-fms tyrosine kinase inhibitor, Ki20227, suppresses osteoclast differentiation and osteolytic bone destruction in a bone metastasis model. *Mol Cancer Ther* 5(11):2634–2643.
44. Ohno H, et al. (2008) The orally-active and selective c-Fms tyrosine kinase inhibitor Ki20227 inhibits disease progression in a collagen-induced arthritis mouse model. *Eur J Immunol* 38(1):283–291.
45. Cummings SR, et al.; FREEDOM Trial (2009) Denosumab for prevention of fractures in postmenopausal women with osteoporosis. *N Engl J Med* 361(8):756–765.
46. Suva LJ, Washam C, Nicholas RW, Griffin RJ (2011) Bone metastasis: Mechanisms and therapeutic opportunities. *Nat Rev Endocrinol* 7(4):208–218.
47. Dai XM, et al. (2002) Targeted disruption of the mouse colony-stimulating factor 1 receptor gene results in osteopetrosis, mononuclear phagocyte deficiency, increased primitive progenitor cell frequencies, and reproductive defects. *Blood* 99(1):111–120.
48. Galli SJ, Kitamura Y (1987) Genetically mast-cell-deficient W/Wv and Sl/Sld mice. Their value for the analysis of the roles of mast cells in biologic responses in vivo. *Am J Pathol* 127(1):191–198.